A Rigorous Solution to the Low-Frequency Breakdown in Full-Wave Finite-Element-Based Analysis of General Problems Involving Inhomogeneous Lossless/Lossy Dielectrics and Nonideal Conductors

Jianfang Zhu, *Student Member, IEEE*, and Dan Jiao, *Senior Member, IEEE*

***Abstract*—Existing methods for solving the low-frequency breakdown problem associated with full-wave solvers rely on low-frequency approximations, which has left a number of research questions to be answered. The conductors are also generally treated as perfect conductors and the dielectric loss is not considered. In this work, a rigorous method that does not utilize low-frequency approximations is developed to eliminate the low frequency breakdown problem for the full-wave finite-element based analysis of general 3-D problems involving inhomogeneous lossless and/or lossy dielectrics and nonideal conductors. This method has been validated by the analysis of realistic on-chip circuits at frequencies as low as dc. Furthermore, it is applicable to both low and high frequencies. In this method, the frequency dependence of the solution to Maxwell's equations is explicitly and rigorously derived from dc to high frequencies. In addition to eliminating the low-frequency breakdown, such a theoretical model of the frequency dependence can be used to understand how the field solution, in a complicated 3-D problem with both lossless/lossy inhomogeneous dielectrics and nonideal conductors, should scale with frequency and at which frequency full-wave effects become important.**

***Index Terms*—Broadband frequency response, electromagnetic analysis, finite-element methods, full-wave analysis, low-frequency breakdown.**

I. Introduction

IT HAS BEEN observed that a full-wave-based solution of Maxwell's equations breaks down at low frequencies [1]–[8]. Such a problem is especially severe in digital and mixed-signal integrated circuit applications in which signals have a wide bandwidth from dc to about the third-harmonic frequency. In these applications, full-wave solvers typically break down at and below tens of megahertz [7], [8], which are right in the range of circuit operating frequencies. Moreover, the low-frequency breakdown problem is also the major contributor to the passivity, stability, and causality issues in frequency-domain models. Therefore, it is of critical importance to solve the low-frequency breakdown problem.

State-of-the-art methods for overcoming the low-frequency breakdown problem can be categorized into two classes. One class of methods is to stitch a static- or quasi-static-based electromagnetic solver with a full-wave-based electromagnetic solver. This approach is inaccurate because static/quasi-static solvers involve fundamental approximations such as decoupled $\mathbf{E}$ and $\mathbf{H}$, which is only true at dc. Moreover, at which frequency to switch between different solvers is an issue. As often seen in practice, the stitched solvers may not reach a consensus at their interfaces. Engineers usually have to employ an approximation-based model to achieve a smooth transition between the static, quasi-static, and full-wave solvers, which artificially introduces another level of inaccuracy. The other class of methods for solving the low-frequency breakdown problem is to extend the validity of full-wave solvers to low frequencies [1]–[8]. These methods have successfully made full-wave solvers capable of handling much lower frequencies. Existing approaches in this category more or less rely on theoretical approximations, at low frequencies. For example, the loop-tree and loop-star basis functions were used to achieve a natural Helmholtz decomposition of the current to overcome the low-frequency breakdown problem in integral-equation-based methods [1]. As another example, the tree-cotree splitting [2] was used to provide an approximate Helmholtz decomposition for edge elements in finite-element-based methods (FEMs). The current-charge integral equations and the augmented electric field integral equation [3], [4] also utilize certain low-frequency approximations that are typically invalid at high frequencies. Calderon preconditioner [5] has been leveraged to stabilize the system of integral equations. However, it has numerical errors at low frequencies [6]. Other methods are inherently built upon low-frequency approximations. These include the methods we developed in [7] and [8].

It is true that, when low-frequency approximations are valid, they can produce accurate results. The question is: given an arbitrary problem, at which frequency are these approximations valid, and to which level of accuracy? In reality, the solution

Manuscript received June 30, 2011; revised September 25, 2011; accepted September 28, 2011. Date of publication November 16, 2011; date of current version December 14, 2011. This work was supported in part by a grant from Intel Corporation, the Office of Naval Research under Award N00014-10-1-0482, and the National Science Foundation under Award 0747578. This paper is an expanded paper from the IEEE International Microwave Symposium, Baltimore, MD, June 5–10, 2011.

The authors are with the School of Electrical and Computer Engineering, Purdue University, West Lafayette, IN 47907 USA (e-mail: djiao@purdue.edu).

Color versions of one or more of the figures in this paper are available online at http://ieeexplore.ieee.org.

Digital Object Identifier 10.1109/TMTT.2011.2171707

to Maxwell's equations is a continuous function of frequency. Theoretically, there does not exist a discontinuity in the electromagnetic spectrum, beyond which full-wave analysis is required and below which quasi-static or static assumptions immediately become valid. As a result, it becomes necessary to find the true solution of Maxwell's equations at low frequencies. Only when the true solution of Maxwell's equations is known at low frequencies can one quantitatively assess the accuracy of various approximations used in existing methods for solving low-frequency problems including static and quasi-static solvers. Such a rigorous solution will also provide answers to critical design questions such as at which frequency full-wave effects become important. Along this line of thought, in [9] and [10], we developed a theoretically rigorous method to eliminate the low-frequency breakdown problem. We showed that the root cause of low-frequency breakdown problem is finite machine precision. To solve the low-frequency breakdown problem, we came up with the idea of transforming the original frequency-dependent deterministic problem to a generalized eigenvalue problem that is frequency-independent. With inexact zero eigenvalues fixed to be exact zeroes, we successfully bypassed the barrier of finite machine precision and solved the low-frequency breakdown problem without fully or partially decoupling $\mathbf{E}$ from $\mathbf{H}$, i.e., utilizing low-frequency approximations.

The method proposed in [9] and [10] only addressed the breakdown problem encountered in the analysis of a purely lossless system containing dielectrics and perfect conductors or a purely lossy system consisting of good conductors only. The problem of finding a rigorous solution to the real-world applications in which nonideal conductors and lossless/lossy dielectrics coexist remains open. Many existing methods for solving the low-frequency breakdown problem in computational electromagnetics treat conductors as perfect conductors. In fact, when low frequencies are considered, one has to account for conductor loss because fields penetrate into conductors at low frequencies. In other words, the skin depth of a conductor becomes comparable to the physical dimension of the conductor. In a system involving both nonideal conductors and dielectrics, the low-frequency breakdown problem is significantly complicated by the frequency-dependent coupling between dielectrics and nonideal conductors. In addition, the physics governing a dielectric is different from that governing a good conductor. For that reason, the solutions in dielectric region and conducting region have different frequency dependences. In addition, the matrix resulting from the analysis of the metal–dielectric composite is highly unbalanced due to the fact that the matrix norm of the block formed inside conductors and that of the block formed outside conductors differ from each other by many orders of magnitude, which further complicates the low-frequency breakdown problem. Moreover, when the dielectric loss is present, the system is further complicated, and, hence, the low-frequency breakdown problem is more difficult to solve. As a result, it becomes a great challenge to overcome the barrier of finite machine precision to develop a rigorous solution of Maxwell's equations for problems involving both nonideal conductors and inhomogeneous lossless/lossy dielectrics.

The major contribution of this paper is a theoretically rigorous method for finding the true solution of Maxwell's equations from high frequencies down to dc for general 3-D electromagnetic problems involving both inhomogeneous lossless/lossy dielectrics and nonideal conductors. The preliminary results were reported in [15]. Here, we complete the method from both theoretical and numerical perspectives. The proposed method does not involve theoretical approximations. Not only is it valid at low frequencies, but it is also valid at high frequencies. To help better convey the proposed idea, we will first present the proposed method for the cases that involve inhomogeneous lossless dielectrics and lossy conductors in Section III. We then show how to incorporate dielectric loss into the proposed method in Section IV. Before that, it is necessary to state the problem and analyze its origin, which is given in Section II.

It is worth mentioning that the proposed rigorous method involves an eigenvalue solution. Although, with advanced techniques, the eigenvalue solutions can also be found in linear complexity [13], [16], the resultant computational cost of solving the low-frequency problem is still not desirable. However, such an eigenvalue solution, in fact, can be avoided because, in the proposed method, the analytical frequency dependence of the solution to Maxwell's equations is explicitly derived from dc to high frequencies. Such an analytical model of the frequency dependence directly suggests a fast full-wave solution that can eliminate the low-frequency breakdown problem in a reduced system of order one, which is detailed in [17]. Such a fast method retains the rigor of the theoretically rigorous solution developed in this work, while eliminating the need for an eigenvalue solution. Without the theoretical model of the frequency response derived from the proposed rigorous solution, the fast and rigorous method in [17] for eliminating the low-frequency breakdown would not be feasible.

In fact, we consider the theoretical model of the frequency dependence of the solution to Maxwell's equations from dc to high frequencies resulting from the proposed rigorous solution as the main outcome of this research work. The use of such a theoretical model of the frequency response goes beyond the elimination of low-frequency breakdown. It can be used to develop a theoretical understanding on how the field solution, in a complicated 3-D problem with both lossless/lossy inhomogeneous dielectrics and nonideal conductors, should scale with frequency, at which frequency full-wave effects become important, at which frequency static assumptions yield good accuracy, and so on.

II. Low-Frequency Breakdown Problem Encountered in the Analysis of a Combined Dielectric and Nonideal Conductor System

Consider a general 3-D electromagnetic problem that involves both inhomogeneous lossless dielectrics and nonideal conductors. A full-wave FEM-based analysis of such a problem results in the following matrix equation in the frequency domain:

$$\mathbf{A}(\omega)x(\omega) = b(\omega) \tag{1}$$

where ω is angular frequency and

$$\mathbf{A}(\omega) = \mathbf{S} - \omega^2\mathbf{T} + j\omega\mathbf{R} \tag{2}$$

in which stiffness matrix $\mathbf{S}$, mass matrix $\mathbf{T}$, and conductivity related mass matrix $\mathbf{R}$ are assembled from their elemental contributions as follows:

$$\begin{aligned}
\mathbf{S}_{ij}^{e} &= \iiint_{V^e} \mu_r^{-1}(\nabla \times \mathbf{N}_i) \cdot (\nabla \times \mathbf{N}_j)\, dV \\
\mathbf{T}_{ij}^{e} &= \iiint_{V^e} \frac{\varepsilon_r}{c^2} \mathbf{N}_i \cdot \mathbf{N}_j\, dV \\
\mathbf{R}_{ij}^{e} &= \iiint_{V^e} \mu_0 \sigma \mathbf{N}_i \cdot \mathbf{N}_j\, dV \\
&\quad + \frac{1}{c} \iint_{S_o} (\hat{n} \times \mathbf{N}_i) \cdot (\hat{n} \times \mathbf{N}_j)\, dS \\
b_i^{e} &= -j\omega\mu_0 \iiint_{V^e} \mathbf{N}_i \cdot \mathbf{J}\, dV. \qquad (3)
\end{aligned}$$

In (3), c is the speed of light in free space, σ is conductivity, ε_r is relative permittivity, $\mathbf{J}$ represents a current source, and $\mathbf{N}$ is the normalized vector basis function used to expand the $\mathbf{E}$ field.

The solution to (1) breaks down at low frequencies. To analyze the low-frequency breakdown problem, we can examine the ratio of $\mathbf{S}$'s norm over $\mathbf{T}$'s norm. From (3), it is clear that, when using a normalized basis $\mathbf{N}$, the value of $\mathbf{S}_{ij}$ is $O(l)$ because $\nabla \times \mathbf{N}$ is proportional to $1/l$, and the value of $\mathbf{T}_{ij}$ is proportional to $10^{-17} l^3$, where l is the average edge length used in a 3-D discretization of an electromagnetic structure. In state-of-the-art VLSI circuits, l is at the level of 1 μm. Hence, the ratio of $\mathbf{T}$'s norm over $\mathbf{S}$'s norm is of the order of 10^{-29}, which is significantly smaller than that in a microwave or millimeter-wave circuit. Since the norm of $\mathbf{T}$ is 10^{-29} smaller than the norm of $\mathbf{S}$ in a VLSI circuit, at low frequencies at which $\omega^2\mathbf{T}$ is 16 orders of magnitude smaller than $\mathbf{S}$, even using double-precision computing, the mass matrix $\mathbf{T}$ is essentially treated as zero by computers when performing the addition of $\omega^2\mathbf{T}$ and $\mathbf{S}$. As a result, the breakdown occurs. The same analysis applies to the ratio of $\mathbf{S}$'s norm over $\mathbf{R}$'s norm. When the contributions of the frequency-dependent terms in (2) cannot be captured correctly, breakdown occurs. In addition, different from a purely dielectric system in which only $\mathbf{T}$ and $\mathbf{S}$ exist, and a purely conducting system in which only $\mathbf{R}$ and $\mathbf{S}$ exist since displacement current can be ignored compared with conduction current, in a system having both dielectrics and lossy conductors, we have to solve the breakdown problem for the combined $\mathbf{T}$, $\mathbf{R}$, and $\mathbf{S}$ system. Since the $\mathbf{T}$-associated term and the $\mathbf{R}$-associated term have different frequency dependences and they also have orders of magnitude difference in magnitude, it is very challenging to capture the effects of both terms at low frequencies to obtain a rigorous solution of Maxwell's equations.

From the analysis above, the root cause of the low-frequency breakdown problem is finite machine precision. Computers always have a finite precision. Apparently, employing static or quasi-static approximations to decouple $\mathbf{E}$ from $\mathbf{H}$ seems to be the only way forward. However, once one employs a static or quasi-static approximation, the accuracy of the resultant solution is questionable. As mentioned earlier, the solution of Maxwell's equations is a continuous function of frequency. In addition to the very low frequencies at which static or quasi-static approximations yield good accuracy and high frequencies where full-wave solutions do not break down, there could exist a range of frequencies in which neither static/quasi-static solvers nor existing full-wave methods can produce accurate results. This range of frequencies is also problem-dependent. In Section III, we show how to rigorously bypass the barrier of the finite machine precision and solve the low-frequency breakdown problem for general problems in which inhomogeneous dielectrics and nonideal conductors coexist. In reality, since the skin depth of a conductor is comparable to the physical dimension of conductors at low frequencies, none of the conductors can be treated as perfect electric conductors when the frequency is low.

The proposed solution preserves the same merits as the theoretically rigorous solution developed in [9] and [10] for problems that involve lossless dielectrics only or lossy conductors only. The proposed solution does not involve theoretical approximations and it avoids switching basis functions. The edge basis that is traditionally used for vector finite-element analysis is employed across all frequencies. It preserves the system matrix. The same mass and stiffness matrices that are constructed in a traditional full-wave FEM solver are used from dc to high frequencies. In addition, the approach is equally applicable to high frequencies in addition to low frequencies.

III. Proposed Rigorous Method for Problems Involving Inhomogeneous Lossless Dielectrics and Nonideal Conductors

Consider a problem that involves both inhomogeneous lossless dielectric materials and nonideal conductors. We divide field unknowns x in (1) into two groups: unknowns outside conductors x_o and unknowns inside conductors x_i. For unknowns that reside on the conducting surface, we categorize them into x_i. The space discretization inside conductors is done in such a way that the rapid field variation within a skin depth can be well captured. The FEM-based system matrix $\mathbf{A}(\omega)$ shown in (1) is correspondingly cast into the following form:

$$\mathbf{A}(\omega) = \begin{bmatrix} \mathbf{A}_{oo}(\omega) & \mathbf{A}_{oi}(\omega) \\ \mathbf{A}_{io}(\omega) & \mathbf{A}_{ii}(\omega) \end{bmatrix} \qquad (4)$$

where

$$\begin{aligned}
\mathbf{A}_{oo}(\omega) &= \mathbf{S}_{oo} - \omega^2 \mathbf{T}_{oo} \\
\mathbf{A}_{oi}(\omega) &= \mathbf{S}_{oi} - \omega^2 \mathbf{T}_{oi} \\
\mathbf{A}_{io}(\omega) &= \mathbf{S}_{io} - \omega^2 \mathbf{T}_{io} \\
\mathbf{A}_{ii}(\omega) &= \mathbf{S}_{ii} + j\omega \mathbf{R}_{ii} - \omega^2 \mathbf{T}_{ii}. \qquad (5)
\end{aligned}$$

Based on the matrix inversion lemma [11], the inverse of (4) can be written as

$$\mathbf{A}(\omega)^{-1} = \begin{bmatrix} \mathbf{A}_{oo}^{-1} + \mathbf{A}_{oo}^{-1}\mathbf{A}_{oi}\tilde{\mathbf{A}}_{ii}^{-1}\mathbf{A}_{io}\mathbf{A}_{oo}^{-1} & -\mathbf{A}_{oo}^{-1}\mathbf{A}_{oi}\tilde{\mathbf{A}}_{ii}^{-1} \\ -\tilde{\mathbf{A}}_{ii}^{-1}\mathbf{A}_{io}\mathbf{A}_{oo}^{-1} & \tilde{\mathbf{A}}_{ii}^{-1} \end{bmatrix} \qquad (6)$$

where

$$\tilde{\mathbf{A}}_{ii} = \mathbf{A}_{ii} - \mathbf{A}_{io}\mathbf{A}_{oo}^{-1}\mathbf{A}_{oi} \qquad (7)$$

which is a modified $\mathbf{A}_{ii}$ matrix that captures the coupling from what is outside conductors to what is inside. In (6) and (7), the argument ω is omitted for clarification with the understanding that all of the terms in (6) and (7) are frequency-dependent.

From (6), it can be seen clearly that, in order to obtain the solution of $A(\omega)$ rigorously from dc to high frequencies, we need to obtain $\mathbf{A}_{oo}^{-1}, \tilde{\mathbf{A}}_{ii}^{-1}$, and the matrix products $\mathbf{A}_{oo}^{-1}\mathbf{A}_{oi}, \mathbf{A}_{io}\mathbf{A}_{oo}^{-1}$, and $\mathbf{A}_{io}\mathbf{A}_{oo}^{-1}\mathbf{A}_{oi}$ rigorously from dc to high frequencies. Unfortunately, the computation of all of these terms breaks down at low frequencies. In the following subsections, we show how to obtain a rigorous solution for each of them.

A. Computing $\mathbf{A}_{oo}(\omega)^{-1}$ From DC to High Frequencies

As shown in (5), we have

$$\mathbf{A}_{oo}(\omega) = \mathbf{S}_{oo} - \omega^2\mathbf{T}_{oo}. \tag{8}$$

It is an FEM-based system formulated for the dielectric region that is outside conductors. This matrix suffers from low-frequency breakdown when the contribution of $\omega^2\mathbf{T}_{oo}$ is neglected due to finite machine precision. However, this problem can be readily overcome by the theoretically rigorous solution we have developed in [9] and [10]. Basically, the solution of (8) can be obtained by solving the following generalized eigenvalue problem that is frequency-independent

$$\mathbf{S}_{oo}v = \lambda\mathbf{T}_{oo}v \tag{9}$$

where λ is eigenvalue and v is eigenvector. Denoting the diagonal matrix formed by all of the eigenvalues as Λ, and the matrix formed by all of the eigenvectors by V, the inverse of (8) can be explicitly written as

$$\mathbf{A}_{oo}(\omega)^{-1} = V(\Lambda - \omega^2\mathbf{I})^{-1}V^T \tag{10}$$

where $\mathbf{I}$ is an identity matrix. We also point out in [9] and [10] that the eigenvalues of (9) can be divided into two groups: one group is associated with physical dc modes and the null space of $\mathbf{S}_{oo}$, and the other is associated with the resonance frequencies of the 3-D structure being simulated. The first group has zero eigenvalues. However, numerically they cannot be computed as exact zeros. Thus, we need to correct the inexact zeros to exact zeros. With that, (10) becomes

$$\begin{aligned}\mathbf{A}_{oo}(\omega)^{-1} &= (V_0\, V_h)\begin{bmatrix}-\omega^2\mathbf{I} & 0\\ 0 & \Lambda_h - \omega^2\mathbf{I}\end{bmatrix}^{-1}(V_0\, V_h)^T\\ &= -\frac{1}{\omega^2}V_0V_0^T + V_h[\Lambda_h - \omega^2\mathbf{I}]^{-1}V_h^T\end{aligned} \tag{11}$$

where V_0 denotes the eigenvectors corresponding to zero eigenvalues, and V_h and Λ_h denote the eigenvectors and eigenvalues corresponding to nonzero eigenvalues, i.e., higher order modes. The solution of $\mathbf{A}_{oo}(\omega)^{-1}$ shown in (11) is rigorous from dc to high frequencies. In addition, the frequency dependence of $\mathbf{A}_{oo}(\omega)^{-1}$ is explicitly derived, because, in (11), except for ω, all of the other terms are frequency-independent.

In static solvers, the entire system formulated for the dielectric region outside conductors is characterized as a capacitor system. As a result, a static solver only captures the effect of the first term in (11). At a frequency ω where the second term cannot be neglected, clearly, static solvers break down. Suggested by (11), the frequency at which one should consider the effect of the second term is problem-dependent since the eigenvalues Λ_h are problem-dependent. In addition, ignoring the contribution of the second term clearly yields different levels of accuracy at different frequencies. This is the reason why we mentioned in the Introduction that even a static/quasi-static solver needs to be assessed in accuracy at low frequencies as long as the frequency is not zero. As far as full-wave solvers are concerned, although they are capable of capturing the effect of both terms in (11) at high frequencies, they miss the effect of both terms at low frequencies due to the loss of $\omega^2\mathbf{T}_{oo}$ term and, hence, breaking down.

B. Computing $\mathbf{A}_{oo}(\omega)^{-1}\mathbf{A}_{oi}(\omega)$ and $\mathbf{A}_{io}(\omega)\mathbf{A}_{oo}(\omega)^{-1}$ From DC to High Frequencies

From (11) and (5), we have

$$\begin{aligned}&\mathbf{A}_{oo}(\omega)^{-1}\mathbf{A}_{oi}(\omega)\\ &\quad= \left[-\frac{1}{\omega^2}V_0V_0^T + V_h[\Lambda_h - \omega^2\mathbf{I}]^{-1}V_h^T\right](\mathbf{S}_{oi} - \omega^2\mathbf{T}_{oi}).\end{aligned} \tag{12}$$

To avoid low-frequency breakdown in the computation of (12), here, we have to realize an important property that is

$$V_0^T\mathbf{S}_{oi} = (\mathbf{S}_{io}V_0)^T = 0. \tag{13}$$

To explain, the eigenvectors V_0, i.e., electric field distribution V_0, corresponding to zero eigenvalues satisfy

$$\mathbf{S}_{oo}V_0 = 0 \tag{14}$$

which can be seen from (9). Each row of the matrix-vector multiplication $\mathbf{S}_{oo}V_0$ is an assembled

$$\mu_r^{-1}\langle\nabla\times\mathbf{N}_{o,j}, \nabla\times\mathbf{E}_o\rangle \tag{15}$$

where $\mathbf{N}_{o,j}$ is the jth vector basis in the region outside conductors, $\nabla\times\mathbf{E}_o$ is the curl of the electric field in the element where $\mathbf{N}_{o,j}$ is located, and the inner product $\langle\,\rangle$ denotes a volume integral in the same element. Hence, the nonzero solution of (14) must satisfy $\nabla\times\mathbf{E}_o = 0$ and thereby be a gradient field. Since V_0 is a gradient field and each row of the matrix-vector multiplication $\mathbf{S}_{io}V_0$ is nothing but an assembled

$$\mu_r^{-1}\langle\nabla\times N_{i,j}, \nabla\times\mathbf{E}_o\rangle \tag{16}$$

where $N_{i,j}$ is the jth vector basis on the conducting surface, we have

$$\mathbf{S}_{io}V_0 = 0 \tag{17}$$

and hence (13). As a result, when computing (12), we should make $V_0V_0^T\mathbf{S}_{oi}$ vanish. We thus obtain

$$\begin{aligned}&\mathbf{A}_{oo}(\omega)^{-1}\mathbf{A}_{oi}(\omega)\\ &\quad= V_0V_0^T\mathbf{T}_{oi} + V_h(\Lambda_h - \omega^2\mathbf{I})^{-1}V_h^T(\mathbf{S}_{oi} - \omega^2\mathbf{T}_{oi}).\end{aligned} \tag{18}$$

It is very important to zero out $V_0V_0^T\mathbf{S}_{oi}$, because otherwise we will have $-(1)/(\omega^2)V_0V_0^T\mathbf{S}_{oi}$ left in (18) instead of $V_0V_0^TT_{oi}$, since the contribution of $\omega^2\mathbf{T}_{oi}$ will be overwhelmed by $\mathbf{S}_{oi}$ at low frequencies, leading to a completely wrong frequency dependence. Again, in (18), only ω is related to frequency, and none of the other terms depend on frequency. Therefore, the frequency dependence of $\mathbf{A}_{oo}(\omega)^{-1}\mathbf{A}_{oi}(\omega)$ is also explicitly derived.

The $\mathbf{A}_{io}(\omega)\mathbf{A}_{oo}(\omega)^{-1}$ can be obtained by taking the transpose of (18).

C. Computing $\mathbf{A}_{io}(\omega)\mathbf{A}_{oo}(\omega)^{-1}\mathbf{A}_{oi}(\omega)$ From DC to High Frequencies

To compute $\mathbf{A}_{io}(\omega)\mathbf{A}_{oo}(\omega)^{-1}\mathbf{A}_{oi}(\omega)$, we use (18) and the third row in (5) to thus obtain

$$\begin{aligned}\mathbf{A}_{io}(\omega)\mathbf{A}_{oo}(\omega)^{-1}\mathbf{A}_{oi}(\omega) = &(\mathbf{S}_{io}-\omega^2\mathbf{T}_{io})\\ &\times\left[V_0V_0^T\mathbf{T}_{oi}+V_h(\Lambda_h-\omega^2\mathbf{I})^{-1}\right.\\ &\left.\times V_h^T(\mathbf{S}_{oi}-\omega^2\mathbf{T}_{oi})\right].\end{aligned}\tag{19}$$

Once again, it is important to utilize the property (13) to make the $\mathbf{S}_{io}V_0V_0^T\mathbf{T}_{oi}$ term vanish, from which we get

$$\begin{aligned}\mathbf{A}_{io}(\omega)\mathbf{A}_{oo}(\omega)^{-1}\mathbf{A}_{oi}(\omega) = &-\omega^2\mathbf{T}_{io}V_0V_0^T\mathbf{T}_{oi}\\ &+(\mathbf{S}_{io}-\omega^2\mathbf{T}_{io})V_h\\ &\times(\Lambda_h-\omega^2\mathbf{I})^{-1}V_h^T(\mathbf{S}_{oi}-\omega^2\mathbf{T}_{oi}).\end{aligned}\tag{20}$$

D. Rigorous Solution of $\tilde{\mathbf{A}}_{ii}(\omega)$ From DC to High Frequencies

The $\tilde{\mathbf{A}}_{ii}(\omega)$ can be written as

$$\tilde{\mathbf{A}}_{ii}(\omega)=\mathbf{S}_{ii}+j\omega\mathbf{R}_{ii}-\omega^2\mathbf{T}_{ii}-\mathbf{A}_{io}(\omega)\mathbf{A}_{oo}(\omega)^{-1}\mathbf{A}_{oi}(\omega).\tag{21}$$

Since, inside the conductors, the displacement current carried by the $\omega^2\mathbf{T}_{ii}$ is many orders of magnitude smaller than the conduction current characterized by the $j\omega\mathbf{R}_{ii}$ term for all of the nonzero frequencies that are currently used in circuit design, (21) can be computed as

$$\tilde{\mathbf{A}}_{ii}(\omega)=\mathbf{S}_{ii}+j\omega\mathbf{R}_{ii}-\mathbf{A}_{io}(\omega)\mathbf{A}_{oo}(\omega)^{-1}\mathbf{A}_{oi}(\omega).\tag{22}$$

Substituting (20) into (22), at low frequencies, we obtain

$$\tilde{\mathbf{A}}_{ii}(\omega)=\mathbf{S}_{ii}+j\omega\mathbf{R}_{ii}-\mathbf{S}_{io}V_h(\Lambda_h)^{-1}V_h^T\mathbf{S}_{oi}\tag{23}$$

which can be rewritten as

$$\tilde{\mathbf{A}}_{ii}(\omega)=\tilde{\mathbf{S}}_{ii}+j\omega\mathbf{R}_{ii}\tag{24}$$

where

$$\tilde{\mathbf{S}}_{ii}=\mathbf{S}_{ii}-\mathbf{S}_{io}V_h(\Lambda_h)^{-1}V_h^T\mathbf{S}_{oi}.\tag{25}$$

The solution of (24) also breaks down at low frequencies. This is because, when frequency is low, the contribution from the frequency-dependent term $j\omega\mathbf{R}_{ii}$ is ignored by computers due to finite machine precision. The $\tilde{\mathbf{A}}_{ii}(\omega)$ thus becomes $\tilde{\mathbf{S}}_{ii}$, which is a rank-deficient matrix (the proof is given in Section III-F). To overcome this problem, similar to the solution of $\mathbf{A}_{oo}(\omega)$, we can first solve the following generalized eigenvalue problem that is frequency-independent:

$$\tilde{\mathbf{S}}_{ii}x=\lambda_{ii}\mathbf{R}_{ii}x.\tag{26}$$

Since $\tilde{\mathbf{S}}_{ii}$ is symmetric, as can be seen from (25), and $\mathbf{R}_{ii}$ is positive definite due to the fact that it is a mass matrix, (26) is said to be a symmetric positive definite generalized eigenvalue problem [12], which is the same as (9). For this class of problem, the eigenvectors are both $\tilde{\mathbf{S}}_{ii}$- and $\mathbf{R}_{ii}$-orthogonal. Denoting the matrix formed by all of the eigenvectors of (26) by V_{ii}, we have $V_{ii}^T\mathbf{R}_{ii}V_{ii}=\mathbf{I}$ if the eigenvectors are normalized with respect to $\mathbf{R}_{ii}$. The inverse of $\tilde{\mathbf{A}}_{ii}(\omega)$ shown in (24) can then be rigorously obtained as

$$\tilde{\mathbf{A}}_{ii}(\omega)^{-1}=V_{ii}(\Lambda_{ii}+j\omega\mathbf{I})^{-1}V_{ii}^T\tag{27}$$

where Λ_{ii} is a diagonal matrix consisting of all of the eigenvalues. Since $\tilde{\mathbf{S}}_{ii}$ is obtained numerically from computing (25), it may not be kept strictly symmetric due to numerical roundoff errors. As a result, $V_{ii}^T\mathbf{R}_{ii}V_{ii}$ becomes not strictly diagonal. In this case, one could enforce $\tilde{\mathbf{S}}_{ii}$ to be symmetric before solving the eigenvalue problem (26) or obtaining the inverse of $\tilde{\mathbf{A}}_{ii}(\omega)$ from the following formula:

$$\tilde{\mathbf{A}}_{ii}(\omega)^{-1}=V_{ii}(\Lambda_{ii}+j\omega\mathbf{I})^{-1}(V_{ii}^T\mathbf{R}_{ii}V_{ii})^{-1}V_{ii}^T.$$

The zero eigenvalues of (26) cannot be computed as exact zeros either. We thus fix them to be exact zeros, from which we obtain

$$\begin{aligned}\tilde{\mathbf{A}}_{ii}(\omega)^{-1}&=(V_{ii,0}\,V_{ii,h})\begin{bmatrix}j\omega\mathbf{I} & 0\\ 0 & \Lambda_{ii,h}+j\omega\mathbf{I}\end{bmatrix}^{-1}(V_{ii,0}\,V_{ii,h})^T\\ &=\frac{1}{j\omega}V_{ii,0}V_{ii,0}^T+V_{ii,h}[\Lambda_{ii,h}+j\omega\mathbf{I}]^{-1}V_{ii,h}^T\end{aligned}\tag{28}$$

where $V_{ii,0}$ denotes the eigenvectors corresponding to zero eigenvalues, and $V_{ii,h}$ denotes those corresponding to nonzero ones.

E. Final Solution

From the previous four sections, we obtain $\mathbf{A}_{oo}^{-1}$, $\tilde{\mathbf{A}}_{ii}^{-1}$, and the matrix products $\mathbf{A}_{oo}^{-1}\mathbf{A}_{oi}$, $\mathbf{A}_{io}\mathbf{A}_{oo}^{-1}$, and $\mathbf{A}_{io}\mathbf{A}_{oo}^{-1}\mathbf{A}_{oi}$ rigorously from dc to high frequencies. Substituting them into (6), we obtain the solution of (1), which can be written as

$$\begin{aligned}x(\omega)&=\mathbf{A}(\omega)^{-1}b(\omega)\\ &=\begin{bmatrix}(\mathbf{A}^{-1})_{oo} & (\mathbf{A}^{-1})_{oi}\\ (\mathbf{A}^{-1})_{io} & (\mathbf{A}^{-1})_{ii}\end{bmatrix}\begin{Bmatrix}b_o\\ b_i\end{Bmatrix}\end{aligned}\tag{29}$$

where

$$\begin{aligned}(\mathbf{A}^{-1})_{oo}&=\mathbf{A}_{oo}(\omega)^{-1}+\mathbf{A}_{oo}(\omega)^{-1}\mathbf{A}_{oi}(\omega)\\ &\quad\times\tilde{\mathbf{A}}_{ii}(\omega)^{-1}\mathbf{A}_{io}(\omega)\mathbf{A}_{oo}(\omega)^{-1}\\ (\mathbf{A}^{-1})_{oi}&=-\mathbf{A}_{oo}(\omega)^{-1}\mathbf{A}_{oi}(\omega)\tilde{\mathbf{A}}_{ii}(\omega)^{-1}\\ (\mathbf{A}^{-1})_{io}&=-\tilde{\mathbf{A}}_{ii}(\omega)^{-1}\mathbf{A}_{io}(\omega)\mathbf{A}_{oo}(\omega)^{-1}\\ (\mathbf{A}^{-1})_{ii}&=\tilde{\mathbf{A}}_{ii}(\omega)^{-1}.\end{aligned}\tag{30}$$

Substituting (11), (18), (20), and (28) into (30), we have

$$\begin{aligned}(\mathbf{A}^{-1})_{ii} &= \frac{1}{j\omega}V_{ii,0}V_{ii,0}^T + V_{ii,h}[\Lambda_{ii,h} + j\omega\mathbf{I}]^{-1}V_{ii,h}^T \\ (\mathbf{A}^{-1})_{oi} &= -\left[V_0V_0^T\mathbf{T}_{oi} + V_h(\Lambda_h - \omega^2\mathbf{I})^{-1}V_h^T \right. \\ &\qquad \left. \times(\mathbf{S}_{oi} - \omega^2\mathbf{T}_{oi})\right](\mathbf{A}^{-1})_{ii} \\ (\mathbf{A}^{-1})_{io} &= (\mathbf{A}^{-1})_{oi}^T \\ (\mathbf{A}^{-1})_{oo} &= -\frac{1}{\omega^2}V_0V_0^T + V_h[\Lambda_h - \omega^2\mathbf{I}]^{-1}V_h^T \\ &\quad - (\mathbf{A}^{-1})_{oi}\left[V_0V_0^T\mathbf{T}_{oi} + V_h(\Lambda_h - \omega^2\mathbf{I})^{-1}\right. \\ &\qquad \left. \times V_h^T(\mathbf{S}_{oi} - \omega^2\mathbf{T}_{oi})\right]^T. \end{aligned} \tag{31}$$

In (31), except for ω, all of the other terms are frequency-independent. Clearly, the solution we obtain is a continuous function of frequency. The frequency dependence of the solution to Maxwell's equations is thus revealed by the proposed method for general 3-D problems that involve both inhomogeneous dielectrics and nonideal conductors. One can rely on it to obtain a rigorous field solution from dc to high frequencies. One can also use it to rigorously assess the accuracy of any low-frequency approximation and answer critical design questions such as when full-wave effects become important.

Although the final solution shown in (31) has a long formula, it has a clear physical meaning. To give an example, consider a common excitation used in the FEM-based analysis of circuits, which is a current probe launched between a reference ground and an active port located in the region outside conductors. The right-hand-side vector b becomes $b = \{-j\omega I \quad 0\}^T$. Then, from (29) and (31), at very low frequencies, the field solution inside conductors x_i and that outside conductors x_o can be explicitly written as

$$\begin{aligned} x_o &= \left(-\frac{1}{\omega^2}V_0V_0^T + \frac{1}{j\omega}\mathbf{Q}V_{ii,0}V_{ii,0}^T\mathbf{Q}^T\right)(-j\omega I) \\ x_i &= -\frac{1}{j\omega}V_{ii,0}V_{ii,0}^T\mathbf{Q}^T(-j\omega I) \end{aligned} \tag{32}$$

where $\mathbf{Q} = V_0V_0^T\mathbf{T}_{oi} + V_h(\Lambda_h)^{-1}V_h^T\mathbf{S}_{oi}$. In the above, again, except for ω, all of the other terms are frequency-independent. It is clear that, given a constant current excitation I, the x_o has a constant real part and an imaginary part that is inversely proportional to frequency, which agrees with our physical understanding that the electric field solution outside conductors is dominated by *RC* effects at very low frequencies. On the other hand, the x_i is a constant real number, which also agrees with physics: the voltage drop along each edge inside a conductor is a constant given a constant current excitation. In addition, (32) yields a rigorous solution at dc. At dc, x_o is shown to have a constant real part and an infinitely large imaginary part, and x_i is shown to be a constant real number. This is consistent with the fact that the nonideal conductor has a resistance and the capacitance formed between conductors becomes an open circuit at dc.

F. Existence of Zero Eigenvalues of $\tilde{\mathbf{S}}_{ii}$

As can be seen from (25), the $\tilde{\mathbf{S}}_{ii}$ is composed of $\mathbf{S}_{ii}$ and $-\mathbf{S}_{io}V_h(\Lambda_h)^{-1}V_h^T\mathbf{S}_{oi}$. $\mathbf{S}_{ii}$ is a stiffness matrix. However, it is different from the stiffness matrix that is constructed solely for a conducting region, which is denoted by $\mathbf{S}_{ii,c}$. In fact, $\mathbf{S}_{ii,c}$ is only one component of $\mathbf{S}_{ii}$. Additionally, $\mathbf{S}_{ii}$ is supplemented by $\mathbf{S}_{ii,b}$ denoting the contribution from the elements that are external to conductors and also adjacent to the conductors, as shown in [8, Fig. 7], which is copied in Fig. 1 for clarity. Therefore, $\tilde{\mathbf{S}}_{ii}$ can be decomposed into three terms, which is shown as follows:

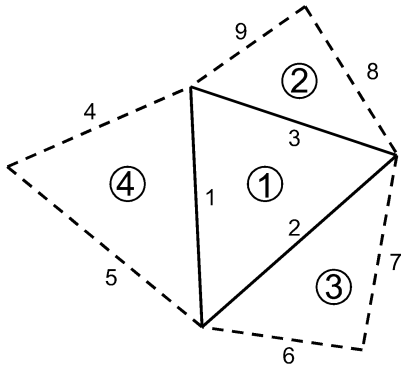

Fig. 1. Mesh with element 1 in the conducting region and the other three elements in the dielectric region (after [8]).

$$\tilde{\mathbf{S}}_{ii} = \mathbf{S}_{ii,c} + \mathbf{S}_{ii,b} - \mathbf{S}_{io}V_h(\Lambda_h)^{-1}V_h^T\mathbf{S}_{oi}. \tag{33}$$

Finding the null space of $\tilde{\mathbf{S}}_{ii}$ is equivalent to finding a nonzero solution x_i that satisfies the following equation:

$$\tilde{\mathbf{S}}_{ii}x_i = 0 \tag{34}$$

which is

$$\mathbf{S}_{ii,c}x_i + \mathbf{S}_{ii,b}x_i - \mathbf{S}_{io}V_h(\Lambda_h)^{-1}V_h^T\mathbf{S}_{oi}x_i = 0. \tag{35}$$

Since $\mathbf{S}_{ii,c}$ is the stiffness matrix that represents the system for conductors only, it is known to have a null space. Hence, there exists a gradient field solution x_i satisfying $\mathbf{S}_{ii,c}x_i = 0$. In contrast, $\mathbf{S}_{ii}$ may have no null space; instead, it can be positive definite due to the addition of $\mathbf{S}_{ii,c}$ with $\mathbf{S}_{ii,b}$. However, in $\tilde{\mathbf{S}}_{ii}$, the $-\mathbf{S}_{io}V_h(\Lambda_h)^{-1}V_h^T\mathbf{S}_{oi}$ term, which captures the coupling from what is outside conductors to what is inside, counteracts the contribution from $\mathbf{S}_{ii,b}$, hence inducing a null space of $\tilde{\mathbf{S}}_{ii}$. Therefore, the nonzero solution of (35) can be found, which is a gradient field. This agrees with the physics that the system inside the conductor also has dc modes. The above analysis could be conceptual. Next, we give a quantitative analysis.

Equation (35) is in fact

$$\mathbf{S}_{ii,c}x_i + \mathbf{S}_{ii,b}x_i + \mathbf{S}_{io}x_o' = 0 \tag{36}$$

where x_o' is the field solution outside conductors at dc. This is because, at dc, since both b_o and b_i are zero, from (1) and (4) we obtain

$$(\mathbf{A}_{ii} - \mathbf{A}_{io}\mathbf{A}_{oo}^{-1}\mathbf{A}_{oi})x_i = 0. \tag{37}$$

Substituting $\omega = 0$ into the $\mathbf{A}_{ii}$ given in (5) and $\mathbf{A}_{io}\mathbf{A}_{oo}^{-1}\mathbf{A}_{oi}$ shown in (20), we obtain (35), where $-V_h(\Lambda_h)^{-1}V_h^T\mathbf{S}_{oi}x_i$ is nothing but $-(\mathbf{A}_{oo}^{-1}\mathbf{A}_{oi})x_i$ at dc, which is x_o'. If we use $\tilde{x}_o$ to

denote the union of the field solution outside conductors and that on the nonideal conducting surface, we can rewrite (36) as

$$\mathbf{S}_{ii,c}x_i + \tilde{\mathbf{S}}_{io}\tilde{x}_o = 0. \tag{38}$$

In the above, each row of the left-hand side can be written as

$$\sum_{e=1}^{k} \mu_r^{-1} \langle \nabla \times \mathbf{N}, \nabla \times \mathbf{E} \rangle_{V^e} \tag{39}$$

where $\mathbf{N}$ is an edge basis located inside conductors or on the conducting surface, $\nabla \times \mathbf{E}$ is the curl of the electric field inside the element that $\mathbf{N}$ belongs to, and k is the number of elements that share $\mathbf{N}$. No matter where the $\mathbf{N}$ is located, a gradient-field inside conductors and a gradient field outside conductors will naturally vanish (39), and hence satisfy (38) automatically. To be specific, the x_i is the gradient-field solution of the system formed for the conductors that stand alone, while the $\tilde{x}_o$ is the gradient-field solution of the system formed for the dielectric region with the nonideal conductor surface being its boundary. Thus, we find the nonzero solution of (38) and thereby the nonzero solution of (34). As a result, the null space of $\tilde{\mathbf{S}}_{ii}$ is found, i.e., $\tilde{\mathbf{S}}_{ii}$ has zero eigenvalues.

The aforementioned theoretical analysis is further verified by numerical experiments, which proved that $\mathbf{S}_{ii,c}$ and $\tilde{\mathbf{S}}_{ii}$ share the same null space. The detailed numerical verification is as follows. When we formulate the system matrix in (1), we also directly construct the corresponding $\mathbf{S}_{ii,c}$ in (33), i.e., the stiffness matrix formed for conducting regions only. We then perform eigenanalysis on both $\mathbf{S}_{ii,c}$ and $\tilde{\mathbf{S}}_{ii}$ and obtain their eigenvectors corresponding to zero eigenvalues, respectively. Let the matrix formed by the eigenvectors corresponding to zero eigenvalues in $\mathbf{S}_{ii,c}$ be $\mathbf{W}_1$, and that in $\tilde{\mathbf{S}}_{ii}$ be $\mathbf{W}_2$. Since any linear combination of null-space eigenvectors also resides in the same null space, $\mathbf{W}_1$ and $\mathbf{W}_2$ may differ a lot in elements. However, we have numerically verified that $\mathbf{W}_2$ satisfies $\mathbf{S}_{ii,c}\mathbf{W}_2 = 0$ in the same manner as $\mathbf{W}_1$ satisfies $\mathbf{S}_{ii,c}\mathbf{W}_1 = 0$. In other words, $\mathbf{W}_2$, which is the null space of $\tilde{\mathbf{S}}_{ii}$, is also the null space of $\mathbf{S}_{ii,c}$. Similarly, the $\mathbf{W}_1$ is also found to satisfy $\tilde{\mathbf{S}}_{ii}\mathbf{W}_1 = 0$.

The other numerical proof we have done is to replace $\tilde{\mathbf{S}}_{ii}$ with $\mathbf{S}_{ii,c}$ when solving (26) for finding its null space $V_{ii,0}$. In other words, instead of solving (26), we solve the following eigenvalue problem:

$$\mathbf{S}_{ii,c}x = \lambda_{ii}\mathbf{R}_{ii}x. \tag{40}$$

Denoting the eigenvectors of the above corresponding to zero eigenvalues by $W_{ii,0}$, we found the following relationship:

$$V_{ii,0}V_{ii,0}^T = W_{ii,0}W_{ii,0}^T. \tag{41}$$

Their relative difference is shown to be as small as 10^{-11} in our numerical tests. This fact further verifies that $\mathbf{S}_{ii,c}$ and $\tilde{\mathbf{S}}_{ii}$ share the same null space in common. Because of this fact, any vector in $V_{ii,0}$ is a linear combination of the vectors in $W_{ii,0}$, thus we have

$$V_{ii,0} = W_{ii,0}\mathbf{Z} \tag{42}$$

where $\mathbf{Z}$ is a full-rank matrix. Since $V_{ii,0}$ is an eigenvector of (26) which is $\mathbf{R}_{ii}$-orthogonal, we have

$$V_{ii,0}^T\mathbf{R}_{ii}V_{ii,0} = \mathbf{I}. \tag{43}$$

Similarly, since $W_{ii,0}$ is an eigenvector of (40), which is also $\mathbf{R}_{ii}$- orthogonal, we have

$$W_{ii,0}^T\mathbf{R}_{ii}W_{ii,0} = \mathbf{I}. \tag{44}$$

Substituting (42) into (43) and utilizing (44), we immediately obtain

$$\mathbf{Z}^T\mathbf{Z} = \mathbf{I}. \tag{45}$$

Thus, $\mathbf{Z}$ is an orthogonal matrix. From (42) and (45), we obtain

$$\begin{aligned} V_{ii,0}V_{ii,0}^T &= (W_{ii,0}\mathbf{Z})(W_{ii,0}\mathbf{Z})^T \\ &= W_{ii,0}\mathbf{Z}\mathbf{Z}^T W_{ii,0}^T = W_{ii,0}W_{ii,0}^T. \end{aligned} \tag{46}$$

Therefore, (41) holds true. As a result, in the solution shown in (32), we can replace $V_{ii,0}V_{ii,0}^T$ by $W_{ii,0}W_{ii,0}^T$ without involving any approximation.

To summarize, $\tilde{\mathbf{S}}_{ii}$ does have zero eigenvalues, the number of which is equal to the number of zero eigenvalues in $\mathbf{S}_{ii,c}$. Furthermore, they share the same null space.

G. Remark on Computational Efficiency

Although the focus of this paper is a rigorous full-wave solution that does not break down at low frequencies, to facilitate the application of the proposed method, here, we discuss the computational efficiency of the proposed method. In the theoretical derivation given above, we considered all of the eigenmodes of (9) and (26) without making any approximation. For a fast computation of (31), given a frequency of interest and a required level of accuracy, one only needs to consider a reduced set of modes that have a large weight in the final solution. This can be seen from (10) and (27). The weight of each mode in $\mathbf{A}_{oo}(\omega)^{-1}$ is determined by $1/(\lambda_j - \omega^2)$ where λ_j is the corresponding eigenvalue; the weight of each mode in $\tilde{\mathbf{A}}_{ii}(\omega)^{-1}$ is determined by $1/(\lambda_{ii,j} + j\omega)$, where $\lambda_{ii,j}$ is the corresponding eigenvalue. Assuming that the number of modes is m, the computation of (31) can be performed in $mO(N)$ complexity instead of $O(N^3)$ complexity. This is because what we need to compute is only matrix-vector multiplications since (31) is used to multiply a vector, and the rank of the eigenvector matrix is m. Similarly, when only a few modes are required out of (9) and (26), the eigenvalue solutions can also be found in linear complexity [13], [16].

Moreover, based on the theoretical model of the frequency dependence of the solution to Maxwell's equations derived in this paper, which is shown in (31), one can develop a fast as well as rigorous solution to eliminate the low-frequency breakdown problem without solving an eigenvalue problem, as shown in [17].

IV. Incorporation of Dielectric Loss in the Proposed Rigorous Method

When both conductor and dielectric loss exist, different from (2), the system matrix resulting from a full-wave FEM-based analysis of a 3-D electromagnetic problem becomes

$$\mathbf{A}(\omega) = \mathbf{S} - \omega^2\mathbf{K} + j\omega\mathbf{R} \tag{47}$$

in which

$$\mathbf{K} = \mathbf{T} - j\mathbf{R_d} \tag{48}$$

where $\mathbf{R_d}$ is assembled from its elemental contributions as follows:

$$(\mathbf{R_d})_{ij}^e = \iiint_{V^e} \frac{\varepsilon_r''}{c^2}\mathbf{N}_i \cdot \mathbf{N}_j \, dV \tag{49}$$

where $\varepsilon = \varepsilon_r - j\varepsilon_r''$ is the complex permittivity that is a practical dielectric loss model commonly used in industry. The system matrix shown in (47) hence becomes a complex-valued matrix although it remains symmetric. The matrix elements of $\mathbf{S}, \mathbf{T}$ and $\mathbf{R}$ are the same as shown in (3). $\mathbf{R_d}$ is low rank if the computational domain is only partially filled by lossy dielectrics. The analysis of the root cause of the low-frequency breakdown problem discussed in Section II equally applies to (47). However, due to the existence of $\mathbf{R_d}$, the rigorous solution to the low-frequency breakdown of (47) needs to be updated from the solution developed for (2). First, the solution of $\mathbf{A}_{oo}(\omega)^{-1}$ needs to be updated from (11) to

$$\begin{aligned}\mathbf{A}_{oo}(\omega)^{-1} &= (\mathbf{S}_{oo} - \omega^2\mathbf{K}_{oo})^{-1} \\ &= \left[-\frac{1}{\omega^2}V_0, V_h(\Lambda_h - \omega^2\mathbf{I})^{-1}\right]\tilde{\mathbf{K}}_{oo}^{-1}(V_0, V_h)^T\end{aligned} \tag{50}$$

where $\tilde{\mathbf{K}}_{oo} = V^T\mathbf{K}_{oo}V$, and the eigenvector matrix V and eigenvalues are obtained from the following system:

$$\mathbf{S}_{oo}v = \lambda\mathbf{K}_{oo}v \tag{51}$$

instead of (9). Since K_{oo} is a full-rank matrix and V is made of linearly independent eigenvectors and, hence, invertible, $\tilde{\mathbf{K}}_{oo}^{-1}$ always exists. Consequently, the solutions of $\mathbf{A}_{io}(\omega)\mathbf{A}_{oo}(\omega)^{-1}, \mathbf{A}_{oo}(\omega)^{-1}\mathbf{A}_{oi}(\omega)$ and $\mathbf{A}_{io}(\omega)\mathbf{A}_{oo}(\omega)^{-1}\mathbf{A}_{oi}(\omega)$ all need to be updated, which are given as follows:

$$\begin{aligned}&\mathbf{A}_{io}(\omega)\mathbf{A}_{oo}(\omega)^{-1} \\ &\quad= \left[K_{io}V_0, (\mathbf{S}_{io} - \omega^2 K_{io})V_h(\Lambda_h - \omega^2\mathbf{I})^{-1}\right] \\ &\qquad\times \tilde{\mathbf{K}}_{oo}^{-1}(V_0, V_h)^T \\ &\mathbf{A}_{oo}(\omega)\mathbf{A}_{oi}(\omega)^{-1} = \left[\mathbf{A}_{io}(\omega)\mathbf{A}_{oo}(\omega)^{-1}\right]^T \\ &\mathbf{A}_{io}(\omega)\mathbf{A}_{oo}(\omega)^{-1}\mathbf{A}_{oi}(\omega) \\ &\quad= \left[\mathbf{K}_{io}V_0, (\mathbf{S}_{io} - \omega^2\mathbf{K}_{io})V_h(\Lambda_h - \omega^2\mathbf{I})^{-1}\right] \\ &\qquad\times \tilde{\mathbf{K}}_{oo}^{-1}\left[-\omega^2\mathbf{K}_{io}V_0, (\mathbf{S}_{io} - \omega^2\mathbf{K}_{io})V_h\right]^T.\end{aligned} \tag{52}$$

Again, here, the key step is to zero out $\mathbf{S}_{io}V_0$, which remedies the breakdown problem in computing these three matrix products.

The computation of $\tilde{\mathbf{A}}_{ii}(\omega)$ also needs an update from that developed in Section III-D. Since only conductor loss exists inside the conducting region, at low frequencies we still solve the $\tilde{\mathbf{A}}_{ii}(\omega)$ system as shown in (24). However, $\tilde{\mathbf{S}}_{ii}$ needs to be updated from (25) to the following:

$$\tilde{\mathbf{S}}_{ii} = \mathbf{S}_{ii} - [\mathbf{K}_{io}V_0, \mathbf{S}_{io}V_h(\Lambda_h)^{-1}]\tilde{\mathbf{K}}_{oo}^{-1}[0, \mathbf{S}_{io}V_h]^T \tag{53}$$

where the second term is $\mathbf{A}_{io}(\omega)\mathbf{A}_{oo}(\omega)^{-1}\mathbf{A}_{oi}(\omega)$ at low frequencies. After we solve (26) based on the updated $\tilde{\mathbf{S}}_{ii}$ shown above, we rigorously obtain the inverse of $\tilde{\mathbf{A}}_{ii}$ as

$$\begin{aligned}\tilde{\mathbf{A}}_{ii}(\omega)^{-1} = (V_{ii,0}\, V_{ii,h})&\begin{bmatrix} j\omega\mathbf{I} & 0 \\ 0 & \Lambda_{ii,h} + j\omega\mathbf{I}\end{bmatrix}^{-1} \\ &\times \tilde{\mathbf{R}}_{ii}^{-1}(V_{ii,0}\, V_{ii,h})^T.\end{aligned} \tag{54}$$

where $\tilde{\mathbf{R}}_{ii} = V_{ii}^T\mathbf{R}_{ii}V_{ii}$. The $\tilde{\mathbf{R}}_{ii}$ cannot be reduced to an identity matrix since $\tilde{\mathbf{S}}_{ii}$ is not symmetric, and therefore (26) is no longer a generalized symmetric definite eigenvalue problem. However, since $\mathbf{R}_{ii}$ has a mass matrix form and V_{ii} is full rank, $\tilde{\mathbf{R}}_{ii}$ is always invertible.

With the solution of $\mathbf{A}_{oo}^{-1}, \tilde{\mathbf{A}}_{ii}^{-1}$ and the matrix products $\mathbf{A}_{oo}^{-1}\mathbf{A}_{oi}, \mathbf{A}_{io}\mathbf{A}_{oo}^{-1}$, and $\mathbf{A}_{io}\mathbf{A}_{oo}^{-1}\mathbf{A}_{oi}$ updated shown in the above, we are ready to obtain a rigorous solution of (47) at any frequency. By using (29) and (30) with (50), (52), and (54) substituted into (30), we obtain the final solution.

V. Numerical Results

In order to validate the proposed method, we simulated a number of on-chip and package examples.

A. Realistic Three-Metal-Layer Test-Chip Interconnect

The first example is a three-metal-layer on-chip interconnect structure fabricated using silicon processing technology on a test chip [14]. It involved a 10-μm-wide strip in the M2 layer, one ground plane in the M1 layer, and one ground plane in the M3 layer. The distance of this strip to the M2 returns at the left- and right-hand sides was 50 μm, which is illustrated in [14, Fig. 4]. The strip was 2000 μm long. A current source was launched from the bottom plane to the center M2 wire at the near end of the wire with the far end left open. With the proposed full-wave solution that is valid starting from dc, we are able to extract a correct input impedance at any low frequency. The real and imaginary parts of the input impedance are listed in Table I from dc to 50 GHz. Three methods are compared: the proposed method, the proposed method without correcting the solution of $\tilde{\mathbf{A}}_{ii}(\omega)$ by using the method described in Section III-D, and the conventional full-wave FEM method. Clearly, the proposed method produces correct frequency dependence across the entire band from low to high frequencies, whereas the conventional full-wave solver is wrong at low frequencies. As for the proposed method without correcting the solution of $\tilde{\mathbf{A}}_{ii}(\omega)$, at low frequencies, although the imaginary part is correct, the real part of the input impedance is wrong. This demonstrates the importance of fixing the low-frequency breakdown problem encountered in the solution of $\tilde{\mathbf{A}}_{ii}(\omega)$, although, compared with the breakdown of $\mathbf{A}_{oo}(\omega)$ shown in (8),

TABLE I
INPUT IMPEDANCE OF A TEST-CHIP INTERCONNECT EXTRACTED BY THREE METHODS FROM 50 GHZ DOWN TO DC

Frequency (Hz)	Real Part of the Input Impedance (Ω)			Imaginary Part of the Input Impedance (Ω)		
	Proposed Method	Proposed Method without correcting $\tilde{\mathbf{A}}_{ii}^{-1}$	Conventional Full-wave Method	Proposed Method	Proposed Method without correcting $\tilde{\mathbf{A}}_{ii}^{-1}$	Conventional Full-wave Method
50×10^{9}	0.686233654	0.686177228	0.686177386	-3.675379609	-3.675382274	-3.675382228
10×10^{9}	2.465052685	2.465048708	2.465048681	-2.585540998	-2.585540459	-2.585540623
1×10^{9}	1.64368952	1.643689508	1.643689569	-35.47546814	-35.47546813	-35.4754746
10^{7}	1.628391905	1.62839366382278	1.62816399656908	-3562.681375	-3562.680879	-3569.994824
4×10^{6}	1.6283921026	1.62839218544898	12.3668376940761	-8906.705632	-8906.705420	-9012.11825
10^{5}	1.628391892	1.62839156689845	9631.59238642889	-356268.242	-356268.241	-13478.9904
10^{4}	1.628391891	1.62835923045364	-5774221.33642889	-3562682.42	-3562682.41	-7764961.98
10^{3}	1.628391891	1.62516987213470	-231.924609176796	-35626824.2	-35626824.1	-20005.3151
10^{2}	1.628391891	1.39632228314836	363.459893268376	-356268242	-356268241.5	-18515.1370
10^{1}	1.628391891	0.114307655213246	-3.54220462623064	-3562682420	-3562682420	35.65916933
1	1.628391891	0.00590324257460440	0.0114035893029634	-3.562682e10	-35626824201	-0.22229683
10^{-16}	1.628391891	-4.8828900968e-25	-1.983218295e-13	-3.56e26	-3.56e26	-3.77e-11
10^{-32}	1.628391891	9.23788524822872e-57	-1.515421600738e-51	-3.56e42	-3.56e42	8.11e-32
0	1.628391891	0	0	Open	Open	0

TABLE II
COMPARISON OF INPUT IMPEDANCE GENERATED BASED ON $W_{ii,0}$ AND THAT BASED ON $V_{ii,0}$

Frequency (Hz)	Relative Difference	
	Real Part	Imaginary Part
10^{5}	5.4959e-10	0
1	5.4959e-10	0
10^{-16}	5.4959e-10	0
10^{-32}	5.4959e-10	0

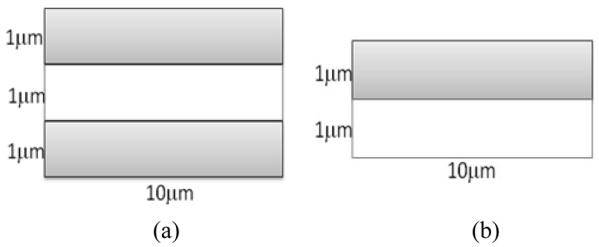

Fig. 2. Cross sectional view of two on-chip parallel-plate interconnects. (a) Structure 1. (b) Structure 2.

the breakdown of $\tilde{\mathbf{A}}_{ii}(\omega)$ shown in (24) is less severe and occurs at a lower frequency. It is worth mentioning that the input impedance is extracted between one port of the interconnect and the bottom reference ground with the other port left open. In Table I, "open" means open circuit.

In addition, for this example, we constructed the corresponding $\mathbf{S}_{ii,c}$ and obtain the eigenvectors of $(\mathbf{S}_{ii,c}, \mathbf{R}_{ii})$ corresponding to zero eigenvalues, which are grouped into $W_{ii,0}$. In Table II, we compare the resultant input impedance based on $W_{ii,0}$ and that based on $V_{ii,0}$ obtained from (26). Besides the same imaginary part, an excellent agreement in the real part can also be observed, as can be seen from Table II, which agrees with the analysis of null space given in Section III-F.

TABLE III
CAPACITANCE SIMULATED BY THE PROPOSED METHOD (C) AND THAT SIMULATED BY THE TRADITIONAL FULL-WAVE FEM SOLVER (C*)

Frequency (Hz)	C* (pF)	C (pF)
1 K	-2.5685e-9	3.0947e-15
1	-0.0033	3.0947e-15
10^{-32}	-2.9804e51	3.0947e-15

TABLE IV
INPUT IMPEDANCE (Ω) SIMULATED BY THE PROPOSED METHOD

Freq (Hz)	Real part		Imaginary part	
	Structure 1	Structure 2	Structure 1	Structure 2
1K	1.1599e-4	5.7996e-5	-5.1429e10	-5.1429e10
1	1.1599e-4	5.7996e-5	-5.1429e13	-5.1429e13
10^{-32}	1.1599e-4	5.7996e-5	-5.1429e45	-5.1429e45
0	1.1599e-4	5.7996e-5	open	open

B. Two Parallel-Plate Structures Made of Lossy Conductors

Second, two parallel-plate examples are simulated, which have analytical solutions. The dimensions of the two structures are $10\times3\times35\ \mu\text{m}^3$, and $10\times2\times35\ \mu\text{m}^3$, respectively, as shown in Fig. 2. The shaded regions are occupied by lossy conductors, the conductivity of which is 5.0×10^{7} S/m. A current source is launched from the bottom plane to the top plane at the near end of the parallel-plate structure. The conventional full-wave FEM solver is shown to break down around 10 MHz, whereas the proposed method generates accurate results down to dc. The analytical capacitances of the two structures are the same, which are known to be 3.0989×10^{-3} pF. In Table III, we compare the capacitance of the first structure simulated by the proposed method and that simulated by a traditional full-wave FEM solver. It is clear that the proposed solution agrees with the analytical data very well, whereas the traditional FEM solver is completely wrong at low frequencies. In addition, we compare the real and imaginary parts of the input impedance of the two structures, which is shown in Table IV. The same imaginary part is obtained at each frequency point for both structures,

TABLE V
INPUT IMPEDANCE (Ω) COMPARISON AT HIGH FREQUENCIES

Freq (GHz)	Real part		Imaginary part	
	Proposed Method	Traditional Solver	Proposed Method	Traditional Solver
1	6.1742e-4	6.1742e-4	-5.1429e4	-5.1429e4
10	1.7820e-2	1.7820e-2	-5.1429e3	-5.1429e3
50	2.7613e-2	2.7613e-2	-1.0285e3	-1.0285e3

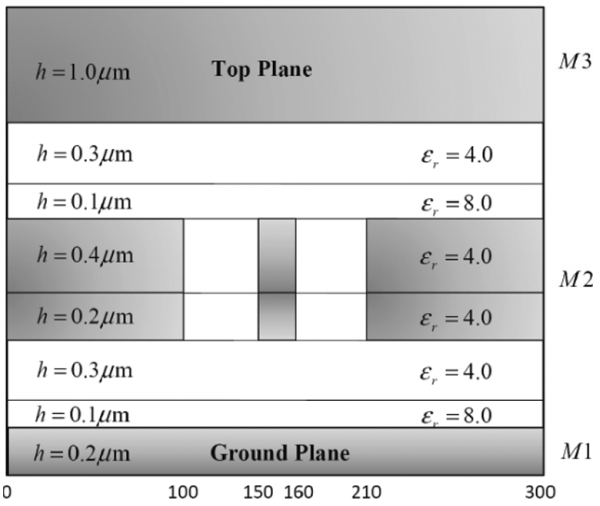

Fig. 3. Illustration of an on-chip 3-D interconnect.

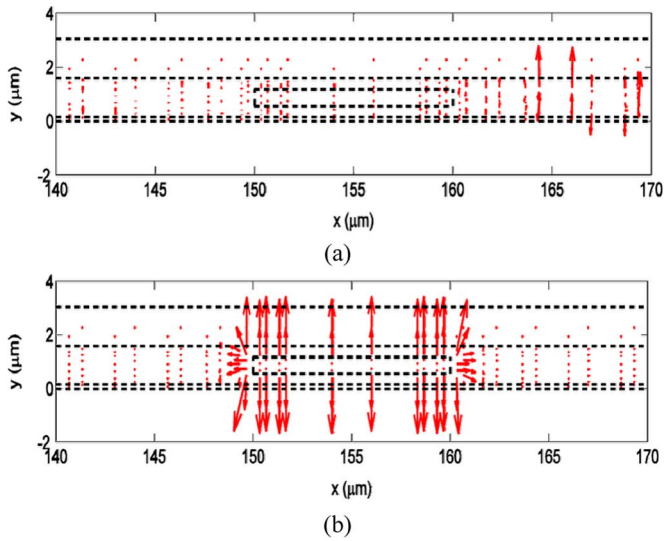

Fig. 4. Simulation of a 3-D on-chip interconnect at 10^{-32} Hz. (a) $\mathbf{E}$ field distribution generated by the conventional FEM method. (b) $\mathbf{E}$ field distribution from the proposed method.

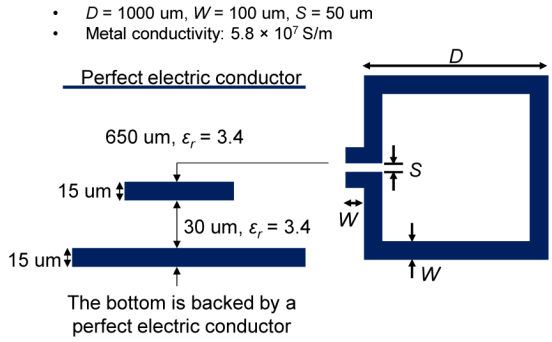

Fig. 5. Geometry and material of a 3-D spiral inductor.

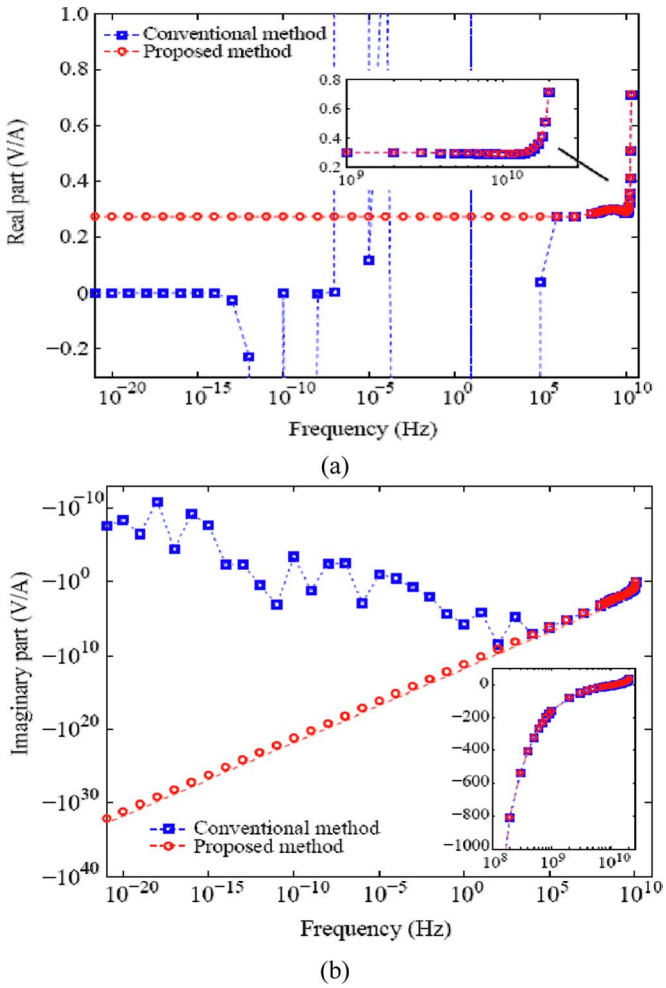

Fig. 6. Comparison of the input impedance of a package inductor simulated by the proposed method and that obtained from a conventional full-wave solver. (a) Real part. (b) Imaginary part.

which agrees with the analytical expectation. Moreover, the analytical resistance of the first structure is shown to be twice as large as that of the second structure, which again shows an excellent agreement with analytical expectation.

The proposed method is not only valid at low frequencies, but also applicable to high frequencies. In Table V, we compare the input impedance of the first lossy parallel-plate structure simulated by the proposed method with that simulated by the conventional full-wave FEM solver at high frequencies. Excellent agreement is observed.

C. A 3-D On-Chip Interconnect

With the proposed method validated, next we simulate another 3-D on-chip interconnect structure, the cross section of which is shown in Fig. 3 with detailed geometry and material data. The conductivity of the metal is 5.8×10^7 S/m. The length of the structure is 2000 μm.

In Fig. 4(a), we plot the $\mathbf{E}$ field distribution at 10^{-32} Hz simulated by a conventional full-wave FEM solver. Clearly, the conventional solver breaks down. In contrast, accurate $\mathbf{E}$ field

TABLE VI
INPUT IMPEDANCE COMPARISON OF A PACKAGE SPIRAL INDUCTOR (Z: INPUT IMPENDENCE; R: RESISTANCE OF THE MICROSTRIP (Ω))

Freq (Hz)	Proposed Full-wave Method			Traditional Full-wave Solver		
	Re[Z]	Im[Z]	R	Re[Z]	Im[Z]	R
10^{5}	4.67754372898e4	-2.6114910093e6	0.056975901	6.52921387922e4	-2.87125821341e6	0.056976147
10^{0}	4.67754229990e9	-2.611491009e11	0.056975898	-0.1809500761171	-91.626878569335	0.057004043
10^{-16}	4.6775422998e25	-2.611491009e27	0.056975898	9.5887449525e-21	-8.8456646786e-14	0.043235684
10^{-32}	4.6775422998e41	-2.611491009e43	0.056975898	3.060297015e-52	-5.45807301936e-30	0.110284028

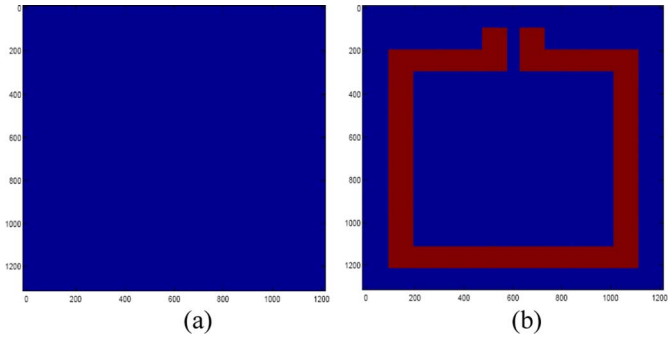

Fig. 7. Simulation of a 3-D spiral inductor at 10^{-32} Hz. (a) Current distribution generated by the conventional full-wave FEM method. (b) Current distribution generated from the proposed method.

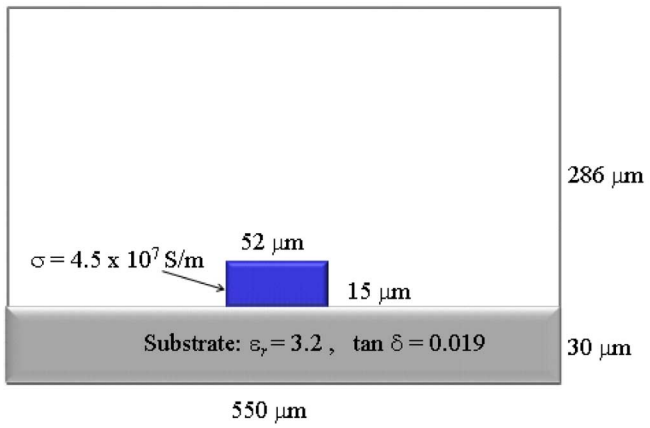

Fig. 8. Package interconnect that has lossy dielectrics and conductors.

distribution is produced by the proposed full-wave method as shown in Fig. 4(b). Moreover, the accuracy of the computed $\mathbf{E}$ field is quantitatively verified. To give an example, the normal component of the electric field in the two dielectric layers above the ground plane is sampled. The ratio between the normal component of the $\mathbf{E}$ field in the layer with relative permittivity 4.0 and that in the layer with relative permittivity 8.0 is 2.015, which agrees very well with the analytical value 2.0. Different from the on-chip interconnect example shown in [9], [10], here, the conductors are not perfect conductors. As can be seen from Fig. 4(a) and (b), there exist fields inside conductors.

D. A 3-D Package Spiral Inductor

The fourth example is a 3-D spiral inductor residing on a package. The geometry of the spiral inductor is shown in Fig. 5. Its diameter (D) is 1000 μm. The metallic wire is 100 μm wide and 15 μm thick. The port separation (S) is 50 μm. The inductor is backed by two package planes. The backplane is 15 μm thick. This structure is simulated successfully by the full-wave-based solver in [14] at high frequencies. In Fig. 6, we compare the input impedance simulated by the proposed method and that obtained from the conventional full-wave method from DC to high frequencies. As can be seen from the insets of Fig. 6(a) and (b), an excellent agreement between the two methods can be observed in both real and imaginary parts of the input impedance at high frequencies. However, the conventional full-wave solution shown in blue breaks down around 1 MHz, which can be clearly seen from two main figures. In contrast, the proposed method can generate correct frequency dependence for both real and imaginary parts at any low frequency. It is clear that the proposed method is able to provide a universal solution to Maxwell's equations from DC to high frequencies. In Fig. 7, we plot the current distribution at 10^{-32} Hz. Clearly, the current simulated by the proposed method agrees with theoretical expectation, while the current generated by the conventional full-wave solver is totally wrong since there is almost no current flowing inside the conductor.

E. Package Interconnect Embedded in Lossy Dielectrics

To demonstrate the capability of the proposed method in solving problems involving both lossy dielectrics and conductors, we simulate a package microstrip-type interconnect that resides on a lossy dielectric substrate having 0.019 loss tangent as shown in Fig. 8. The microstrip has a conductivity of 4.5×10^{7} S/m and is exposed to the air. The results simulated by the proposed method are listed in Table VI in comparison with those from a traditional full-wave solver. Clearly, the traditional solver breaks down at and below 10^{5} Hz. In contrast, the proposed method generates correct input impendence down to dc. Different from lossless dielectric cases, for a lossy dielectric that has a constant loss tangent, the real part of the input impedance should scale with frequency inversely like the imaginary part. This is also suggested by the final solution based on (49), (50), and (53). The proposed method is shown to produce correct frequency dependence, whereas the conventional full-wave solver yields incorrect results. In addition, we extract the resistance of the microstrip, R, from the field solution down to dc. The R is shown to be 0.056975898 Ω, which agrees very well with the analytical dc resistance that is 0.05698 Ω.

VI. CONCLUSION

It has been observed that a full-wave solution of Maxwell's equations breaks down at low frequencies. To overcome the low-frequency breakdown problem, one, also, has to account for

the nonideality of conductors since fields penetrate into conductors at low frequencies. Many existing methods for solving the low-frequency breakdown problem in computational electromagnetics treat conductors as perfect conductors. In addition, in general, they rely on low-frequency approximations to overcome the breakdown problem, which has suggested a number of new research questions to be considered. For example, at which frequency, the low-frequency approximations are valid, and valid to which level of accuracy? Given a frequency, what is the true solution of Maxwell's equations in which $\mathbf{E}$ and $\mathbf{H}$ are coupled as long as frequency is not zero? Static and quasi-static solvers cannot provide a benchmark solution at these breakdown frequencies either since they involve theoretical approximations. Even a quasi-static solution breaks down at low frequencies because of the underlying frequency-dependent system. In reality, the solution to Maxwell's equations is a continuous function of frequency. Theoretically, there does not exist a discontinuity in the frequency spectrum, beyond which full-wave analysis is required and below which quasi-static or static assumptions immediately become valid. The low-frequency breakdown problem is also becoming more and more critical as the smallest feature size of engineering systems is being pushed down to the nanometer regime and beyond while the largest feature size does not scale proportionally.

In order to fundamentally eliminate the low-frequency breakdown problem for the development of both existing and future technology, one has to know the true solution of Maxwell's equations at low frequencies. This paper provides such a true solution for real-world 3-D problems that consist of both inhomogeneous lossless and/or lossy dielectrics and nonideal conductors. This solution also naturally cures the passivity, stability, and causality issues resulted from low-frequency inaccuracy in existing frequency-domain models. In this solution, the frequency dependence of the field solution is explicitly derived from dc to high frequencies. It is a theoretically rigorous solution that constitutes a continuous function of frequency. Such a continuous model does not exist previously since the electromagnetic solvers are traditionally divided into static, quasi-static, and full-wave solvers to cover the full electromagnetic spectrum, and at which frequency to switch between these solvers is not quantitatively known. The proposed method can be employed to quantitatively assess the accuracy of existing electromagnetic solvers at low frequencies including static and quasi-static solvers. In addition, it also provides answers to critical design questions such as at which frequency full-wave effects become important. The proposed method avoids switching basis functions. The edge basis that is traditionally used for vector finite-element analysis is employed across all frequencies. It preserves the system matrix. The same mass and stiffness matrices that are constructed in a traditional full-wave FEM solver are used from dc to high frequencies.

The focus of this paper is a rigorous full-wave solution of Maxwell's equations that does not utilize low-frequency approximations and does not break down at low frequencies. Based on such a rigorous solution, one can develop fast as well as rigorous solutions like the one developed in [17] to eliminate the low-frequency breakdown without solving an eigenvalue problem. Moreover, the application of the proposed rigorous full-wave solution of Maxwell's equations valid from high frequencies down to dc goes beyond the elimination of low-frequency breakdown.

Although the proposed method is developed in the context of the finite-element method, the essential idea is equally applicable to other numerical methods such as finite difference methods and integral-equation-based methods. This is because all of these methods result in a system matrix that can be cast into a form shown in (2), and the proposed method is a general method for analyzing a frequency dependent system like (2) regardless of the origin of the underlying matrices. The matrices that are associated with ω^2, ω, and constant can be generated from either a partial differential equation or an integral equation based solver. Moreover, since the root cause of low-frequency breakdown problem is finite machine precision, the proposed method for bypassing this fundamental barrier can also shed the light on the solution to other unsolved research problems that are caused by finite machine precision.

REFERENCES

[1] J. Zhao and W. C. Chew, "Integral equation solution of Maxwell's equations from zero frequency to microwave frequencies," *IEEE Trans. Antennas Propag.*, vol. 48, no. 10, pp. 1635–1645, Oct. 2000.

[2] S. Lee and J. Jin, "Application of the tree-cotree splitting for improving matrix conditioning in the full-wave finite-element analysis of high-speed circuits," *Microw. Opt. Technol. Lett.*, vol. 50, no. 6, pp. 1476–1481, Jun. 2008.

[3] Z. Qian and W. Chew, "Fast full-wave surface integral equation solver for multiscale structure modeling," *IEEE Trans. Antennas Propag.*, vol. 57, no. 11, pp. 3594–3602, Nov. 2009.

[4] Z. Qian and W. Chew, "Enhanced A-EFIE with perturbation method," *IEEE Trans. Antennas Propag.*, vol. 58, no. 2, pp. 362–372, Feb. 2004.

[5] R. J. Adams, "Physical properties of a stabilized electric field integral equation," *IEEE Trans. Antennas Propag.*, vol. 52, no. 10, pp. 3256–3264, Oct. 2010.

[6] M. B. Stephanson and J.-F. Lee, "Preconditioned electric field integral equation using Calderon identities and dual loop/star basis functions," *IEEE Trans. Antennas Propag.*, vol. 57, no. 4, pp. 1274–1278, Apr. 2009.

[7] J. Zhu and D. Jiao, "A unified finite-element solution from zero frequency to microwave frequencies for full-wave modeling of large-scale three-dimensional on-chip interconnect structures," *IEEE Trans. Adv. Packaging*, vol. 31, no. 4, pp. 873–881, Nov. 2008.

[8] J. Zhu and D. Jiao, "Eliminating the low-frequency breakdown problem in 3-D full-wave finite-element-based analysis of integrated circuits," *IEEE Trans. Microw. Theory Tech.*, vol. 58, no. 10, pp. 2633–2645, Oct. 2010.

[9] J. Zhu and D. Jiao, "A theoretically rigorous solution for fundamentally eliminating the low-frequency breakdown problem in finite-element-based full-wave analysis," in *Proc. IEEE Int. Symp. Antennas Propag.*, Jul. 2010.

[10] J. Zhu and D. Jiao, "A theoretically rigorous full-wave finite-element-based solution of Maxwell's equations from DC to high frequencies," *IEEE Trans. Adv. Packaging*, vol. 33, no. 4, pp. 1043–1050, Nov. 2010.

[11] H. Boltz, "Matrix inversion lemma," 1923. [Online]. Available: http://en.wikipedia.org/wiki/Invertible_matrix,

[12] G. W. Stewart, "Matrix algorithms," *Eigensystems*, vol. II, , pp. 231–240, 2001.

[13] J. Lee, V. Balakrishnan, C.-K. Koh, and D. Jiao, "From $O(k^2N)$ to $O(N)$: A fast complex-valued eigenvalue solver for large-scale on-chip interconnect analysis," *IEEE Trans. Microw. Theory Tech.*, vol. 57, no. 12, pp. 3219–3228, Dec. 2009.

[14] M. J. Kobrinsky, S. Chakravarty, D. Jiao, M. C. Harmes, S. List, and M. Mazumder, "Experimental validation of crosstalk simulations for on-chip interconnects using S-parameters," *IEEE Trans. Adv. Packaging*, vol. 28, no. 1, pp. 57–62, Feb. 2005.

[15] J. Zhu and D. Jiao, "A rigorous solution to the low-frequency breakdown in full-wave finite-element-based analysis of general problems involving inhomogeneous lossy dielectrics and non-ideal conductors," in *Proc. IEEE Int. Microw. Symp.*, Jun. 2011, pp. 1–4.

[16] J. Lee, D. Chen, V. Balakrishnan, C.-K. Koh, and D. Jiao, "A quadratic eigenvalue solver of linear complexity for 3-D electromagnetics-based analysis of large-scale integrated circuits," *IEEE Trans. Comput-Aided Design (CAD) Integr. Syst.*, to be published.

[17] J. Zhu and D. Jiao, "A fast full-wave solution that eliminates the low-frequency breakdown problem in a reduced system of order one," *IEEE Trans. Microw. Theory Tech.*, submitted for publication.

Jianfang Zhu received the B.S. degree in electronic engineering and information science from the University of Science and Technology of China, Hefei, China, in 2006, and the Ph.D. degree in electrical engineering from Purdue University, West Lafayette, IN, in 2011.

She is currently a Senior Engineer with Hard IP Group, Intel Corporation, Santa Clara, CA. Her research interests include computational and applied electromagnetics, high-frequency VLSI design and analysis, multiscale multiphysics modeling, and signal integrity and power integrity analysis.

Dr. Zhu was selected as the Best Student Paper Award finalist in the 2010 IEEE International Symposium on Antennas and Propagation. One of her papers was also among the three finalists of the 2010 IEEE Transactions on Advanced Packaging Best Paper Award. Her dissertation was nominated for Dimitris N. Chorafas Foundation Award for Outstanding Ph.D. Thesis. She was the recipient of the Best Undergraduate Thesis Award and the Outstanding Student Scholarship from theUniversity of Science and Technology of China.

Dan Jiao (S'00–M'02–SM'06) received the Ph.D. degree in electrical engineering from the University of Illinois at Urbana-Champaign, Urbana, in 2001.

She then joined the Technology Computer-Aided Design (CAD) Division, Intel Corporation, until September 2005, as a Senior CAD Engineer, Staff Engineer, and Senior Staff Engineer. In September 2005, she joined Purdue University, West Lafayette, IN, as an Assistant Professor with the School of Electrical and Computer Engineering, where she is now a tenured Associate Professor. She has authored two book chapters and over 140 papers in refereed journals and international conferences. Her current research interests include computational electromagnetics, high-frequency digital, analog, mixed-signal, and RF integrated circuit (IC) design and analysis, high-performance VLSI CAD, modeling of microscale and nanoscale circuits, applied electromagnetics, fast and high-capacity numerical methods, fast time-domain analysis, scattering and antenna analysis, RF, microwave, and millimeter-wave circuits, wireless communication, and bio-electromagnetics.

Dr. Jiao has served as a reviewer for many IEEE journals and conferences. She was among the 100 engineers selected throughout the nation for the National Academy of Engineering's 2011 US Frontiers of Engineering Symposium. She was the 2010 recipient of the Ruth and Joel Spira Outstanding Teaching Award, the 2008 National Science Foundation (NSF) CAREER Award, the 2006 Jack and Cathie Kozik Faculty Start up Award (which recognizes an outstanding new faculty member of the School of Electrical and Computer Engineering, Purdue University), a 2006 Office of Naval Research (ONR) Award under the Young Investigator Program, the 2004 Best Paper Award presented at the Intel Corporation's annual corporate-wide technology conference (Design and Test Technology Conference) for her work on generic broadband model of high-speed circuits, the 2003 Intel Corporation's Logic Technology Development (LTD) Divisional Achievement Award in recognition of her work on the industry-leading BroadSpice modeling/simulation capability for designing high-speed microprocessors, packages, and circuit boards, the Intel Corporation's Technology CAD Divisional Achievement Award for the development of innovative full-wave solvers for high-frequency IC design, the 2002 Intel Corporation's Components Research the Intel Hero Award (Intel-wide she was the tenth recipient) for the timely and accurate 2-D and 3-D full-wave simulations, the Intel Corporation's LTD Team Quality Award for her outstanding contribution to the development of the measurement capability and simulation tools for high-frequency on-chip crosstalk, and the 2000 Raj Mittra Outstanding Research Award presented by the University of Illinois at Urbana-Champaign.